THE JOURNAL OF BIOLOGICAL CHEMISTRY VOL. 280, NO. 51, pp. 42061–42066, December 23, 2005
© 2005 by The American Society for Biochemistry and Molecular Biology, Inc. Printed in the U.S.A.

Kinetics and Template Nucleation of Self-Assembled Hydroxyapatite Nanocrystallites by Chondroitin Sulfate*

Received for publication, October 29, 2004, and in revised form, September 23, 2005 Published, JBC Papers in Press, October 25, 2005, DOI 10.1074/jbc.M412280200

Huaidong Jiang[‡], **Xiang-Yang Liu**[‡1], **Gang Zhang**[§], **and Yang Li**[§]

From the [‡]*Department of Physics, National University of Singapore, 2 Science Drive 3, Singapore 117542 and the* [§]*Department of Biochemistry, National University of Singapore, 8 Medical Drive, Singapore 117597, Singapore*

Biomineralization is an important process, which is often assisted by biomolecules. In this paper, the effect of chondroitin sulfate on the crystallization of hydroxyapatite was examined quantitatively based on a generic heterogeneous nucleation model. It is found that chondroitin sulfate can suppress the supersaturation-driven interfacial structure mismatch between the hydroxyapatite crystal and the substrate and promote the formation of ordered hydroxyapatite nanocrystallite assemblies. The nucleation mechanism of self-aligned hydroxyapatite nanocrystallites was examined from the viewpoints of kinetics and interfacial structure and properties, which contributes to an understanding of the fundamentals of biomineralization of self-assembled structures. The results obtained from this study will provide a basic principle to design and fabricate highly orderly organic-inorganic hybrid materials.

Natural materials such as bones and teeth consist of biocomposites with well organized and assembled hydroxyapatite (HAP[2]; $Ca_5(PO_4)_3OH$) nanobiominerals, to perform important biological functions. Although such composites in hard tissues are formed under mild conditions, they exhibit unusual mechanical properties that outperform synthetic materials (1, 2). How can biomineral nanocrystallites be assembled to form a synergetic structure? Why are some molecules, in particular biomacromolecules, capable of fabricating different patterns of biominerals? Recently, these questions concerning the biological mechanisms that control mineralized tissue construction have attracted a great deal of attention in fields ranging from biology and chemistry to materials science and bioengineering (3–7).

It is well documented that the ordered structures in mineralized tissues appeared to originate from organized assemblies of biomacromolecules, such as proteins, polysaccharides, or proteoglycans, and inorganic compound salts (8–10). Previous studies indicate that some biomacromolecules are involved in controlling the nucleation, growth, size, and shape of the mineral phases (11), since they can act as templates through self-assembly to facilitate interaction with an insoluble matrix and to induce the desired stereochemistry for the construction of organized structures (12, 13). Normally, these molecules are functionalized with acidic groups such as carboxylic acid, sulfonate, and phosphate moieties, which enable them to become an effective metal ion chelator to combine with the inorganic matrix (14–16). Chondroitin 4-sulfate (ChS) is just one of these biomolecules. It belongs to the family of glycosaminoglycans, which can be found on cell surfaces and in the extracellular matrix of cartilage and bone. Large amounts of it in the cartilage permit diffusion of substances between blood and vessels. ChS consists of repeated disaccharide units; one of the two monosaccharides is *N*-acetylgalactosamine sulfate (GalNAc-OSO_3^-), and the other is glucuronic acid that contains a carboxylate group (*cf.* Fig. 1). Previous investigation indicated that ChS is present at the early stages of bone and tooth formation and is considered to be implicated in regulating mineral deposition and crystal morphology in mineralization during osteogenesis (6, 17–19). In addition, ChS may promote healing of bones (20). However, the mechanisms of biomolecule-mediated mineralization, in particular the detailed nucleation kinetic processes and the molecular recognition mechanism at the interface between biomolecule and biomineral, are poorly understood.

In this paper, we present a study on the templating effect of ChS on the nucleation of HAP using a light-scattering technique. A generic kinetic model on nucleation (21) is applied to analyze quantitatively the effect of ChS on HAP crystallization. In the presence of ChS, we synthesized self-aligned HAP nanocrystallites from supersaturated solutions, and here we discuss the nucleation mechanism. We hope this study will not only provide a new and comprehensive understanding of the nucleation mechanism of self-assembled HAP biominerals but also a basic design principle for the development of biocompatible human-made materials.

EXPERIMENTAL PROCEDURES

Nucleation Kinetics Experiments—The nucleation kinetics experiments of HAP were performed on a dynamic light-scattering system (BI-200SM; Brookhaven Instruments Corp.), which can detect particles of a size down to several nanometers and allow an *in situ* measurement of the nucleation process (21). First, two aqueous solutions of $CaCl_2 \cdot 2H_2O$ and $K_2HPO_4 \cdot 3H_2O$ with a molar ratio of 1.67 of calcium/phosphorus were prepared. After determining the range of concentrations in which the nucleation induction time could be detected, a series of concentrations of these two solutions (varying from 2.3 to 3.0 mM for $CaCl_2$) was prepared by diluting the original solutions. Then both kinds of solutions with 10 mg/liter ChS (Sigma) were injected through filters (200 nm) into a glass cell in the dynamic light-scattering system. The kinetics of nucleation could be measured in terms of the nucleation induction time at different supersaturations. In order to study the effect of ChS on the nucleation of HAP, the nucleation kinetics experiments were also performed on the control solutions without additives. In all of the kinetics experiments, the temperature was controlled and fixed at 25 °C.

Preparation of HAP Nanocrystal Self-assemblies—After performing nucleation kinetics experiments, we obtained the HAP precipitation from the supersaturated solutions (the concentrations of $CaCl_2$ and K_2HPO_4 were 2.5 and 1.5 mM, respectively) in the presence and absence of ChS (10 mg/liter). The precipitate was washed with deionized water and acetone, respectively, and subsequently dried. Since several phases were possible during the precipitation of calcium phosphate aggregates from a supersaturated solution (22), x-ray diffraction analyses were car-

* The costs of publication of this article were defrayed in part by the payment of page charges. This article must therefore be hereby marked "*advertisement*" in accordance with 18 U.S.C. Section 1734 solely to indicate this fact.

[1] To whom correspondence should be addressed. Tel.: 65-6874-2812; Fax: 65-6777-6126; E-mail: phyliuxy@nus.edu.sg.

[2] The abbreviations used are: HAP, hydroxyapatite; ChS, chondroitin 4-sulfate; SE, scanning electron.

Downloaded from www.jbc.org at Univ of Ottawa - OCUL, on February 25, 2013

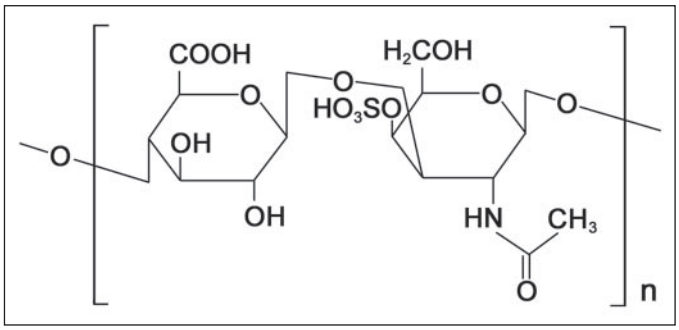

FIGURE 1. **Chemical structure of the repeated disaccharide unit for chondroitin 4-sulfate molecules.**

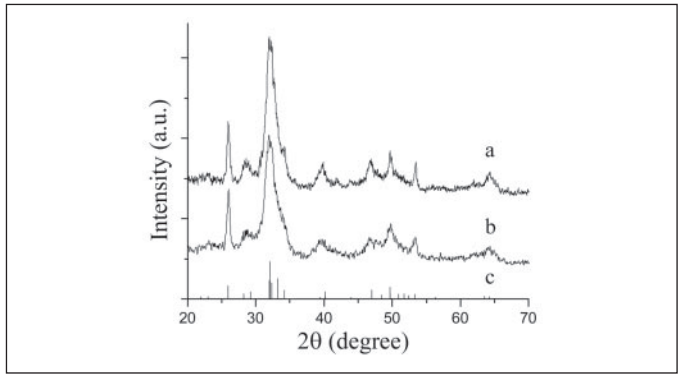

FIGURE 2. **X-ray diffraction patterns of HAP obtained from solutions with no additives (*a*) and HAP obtained from solutions with ChS (*b*) are shown along with the *lines* representing the patterns reported in the JCPDS data base, card number 86-0740 (*c*).** *a.u.*, arbitrary units.

ried out in order to confirm the obtained crystalline phases under the above conditions. The results showed that the samples were mainly hexagonal HAP crystals (*cf.* Fig. 2).

ζ Potential Measurement and Equilibrium Dialysis—As shown in Fig. 1, chondroitin 4-sulfate consists of repeated disaccharide units ($(C_{14}H_{20}O_{14}NS)_n$), which possess acidic groups such as carboxylic and sulfate groups. In order to obtain a good understanding on the electrochemical properties of ChS, a ζ potential measurement of ChS in an aqueous solution with a concentration of 100 mg/liter at pH 6 was performed on a ζ potentiometer (Zetasizer 2000; The Malvern Instruments). Then a series of solutions with ChS and various concentrations of $CaCl_2$ were also measured to study the effect of the calcium ion on the ζ potential of chondroitin sulfate.

Equilibrium dialysis of ChS was performed with the dispo-equilibrium dialyzers, which consist of two chambers separated by a dialysis membrane with a molecular mass cut-off of 5 kDa. The apparatus for equilibrium dialysis was washed with 10 mM EDTA, followed by an extensive wash with deionized water. The upper chambers were filled with ChS solution with a concentration of 100 mg/liter. The bottom chambers were filled with the dialysis buffer containing $CaCl_2$ varying from 10 μM to 3 mM plus trace $^{45}CaCl_2$ (Amersham Biosciences). Dialysis was carried out for 24 h at room temperature, and the radioactivity from ^{45}Ca in the bottom and the upper chambers was measured by using a Beckman LS-6500 liquid scintillation counter. The bound and free Ca^{2+} was then counted, and the dissociation constant K_d was determined by Scatchard analysis (23).

Electron Microscopy and Electron Diffraction—A scanning electron microscope study of the HAP crystallite nanostructure in precipitation was carried out using a scanning electron (SE) microscope (JEOL 6700F, Japan) at 10 kV after coating the sample with platinum to increase the conductivity. The microstructure of the HAP assemblies obtained from the solutions was also observed by using a high resolution transmission electron microscope (JEOL 3010) and electron diffraction techniques.

RESULTS AND DISCUSSION

Kinetic Model for Biomineral Nucleation—In most cases, biomineralization is associated with the formation of a new crystalline phase from the ambient phase via nucleation followed by growth (24). This implies that nucleation, as the first step of biomineralization, plays an important role in building up a complex structure. As we know, a positive thermodynamic driving force is required for HAP crystallization, which is defined as in Ref. 25,

$$\Delta\mu = kT\ln(1+\sigma) = kT\ln\frac{[a(Ca^{2+})]^5[a(PO_4^{3-})]^3[a(OH^-)]}{K_{sp}(HAP)} \quad \text{(Eq. 1)}$$

where k is the Boltzmann constant, T is the absolute temperature, K_{sp} is the solubility product, and $a(i)$ is the activity of species i. σ is defined as the supersaturation of a solution, being the source of a driving force for mineralization in solutions.

In nature, nucleation is under the control of a kinetic process in which HAP nuclei overcome a kinetic barrier, the so-called nucleation barrier (ΔG^*) at a given thermodynamic driving force $\Delta\mu$ (25). Taking into account the effect of the substrate on both the nucleation barrier and the transport process, the nucleation rate is given according to the model (21, 26) as follows,

$$J = (R^s)^2 N^0 f''(m)[f(m)]^{1/2} B \exp\left[-\frac{\Delta G^*_{homo}}{kT} f(m)\right] \quad \text{(Eq. 2)}$$

with

$$\Delta G^*_{homo} = \frac{16\pi\gamma_{cf}^3\Omega^2}{3[kT\ln(1+\sigma)]} \quad \text{(Eq. 3)}$$

and

$$f(m) = \frac{1}{4}(2 - 3m + m^3) \quad \text{(Eq. 4)}$$

where R^s and N^0 are the radius and the density of the substrates, respectively, B is the kinetic constant, ΔG^*_{homo} is the homogeneous nucleation barrier, γ_{cf} is the specific interfacial free energy between the crystals and the mother phase, and Ω is the volume of the growth units. m is a function of the interfacial free energy difference between the phases of crystal, fluid, and substrate, and it depends on the interaction and interfacial structural match between the crystalline phase and the substrate (27).

According to Equation 2, in the presence of substrates the nucleation barrier assumes the following form,

$$\Delta G^* = \Delta G^*_{homo} f(m) \quad (0 \le f \le 1) \quad \text{(Eq. 5)}$$

where $f(m)$ is the interfacial correlation factor describing the lowering of the nucleation barrier ΔG^* due to the occurrence of foreign bodies. Notice that the factor $f(m)$ varies from 0 to 1, depending on the correlation and structure match between the nucleating phase and the substrate (foreign bodies) (28). When the interaction between the nucleating phase and the substrate is optimal, one has $f(m) \to 0$ (*cf.* Equation 4). Conversely, if the interfacial correlation is very poor, one has $f(m) \to 1$,

Downloaded from www.jbc.org at Univ of Ottawa - OCUL, on February 25, 2013

meaning that the substrate exerts almost no influence on the nucleation barrier. Under such conditions, the nucleation of HAP will become very difficult. Obviously, the influence of foreign particles such as dust particles, proteins, or even existing HAP crystallites, etc., on the nucleation barrier, and the association between the nucleating phase and the substrate can be fully characterized by this factor.

Since a direct measurement of the nucleation rate is difficult, to characterize the kinetics of nucleation, one of the most common ways is to measure the nucleation induction time (t_s) at different supersaturations. By definition (21), the nucleation rate J can be expressed as follows,

$$J \cong 1/(t_s V) \quad \text{(Eq. 6)}$$

where V is the volume of the system. Combining Equations 2 and 6 yields the following,

$$\ln t_s = \frac{\kappa f(m)}{[\ln(1+\sigma)]^2} - \ln\{V(R^s)^2 N^0 f''(m)[f(m)]^{1/2} B\} \quad \text{(Eq. 7)}$$

where $\kappa = 16\pi\gamma_{cf}{}^3\Omega^2/3(kT)^3$, which remains constant under a given condition.

It follows then from Equation 7 that for HAP nucleation, the plot $\ln(t_s)$ *versus* $1/[\ln(1+\sigma)]^2$ will give rise to a straight line for a given $f(m)$. As illustrated in Fig. 3, in the case of nucleation promotion (transition from curve 0 to curve 1), the adsorption of additives on the original substrate will lead to a stronger interaction and a better structural match between the substrate and the nucleating phase. This will then result in a decrease of the nucleation barrier. Since for a given nucleation system, κ is constant, such a change can then be identified from the lowering of the slope (corresponding to $\kappa f(m)$) and the increase of the intercept of the $\ln(t_s)$ *versus* $1/[\ln(1+\sigma)]^2$ plot (*cf.* Equation 7). Conversely, if the adsorption of additives leads to repulsion and an interfacial structure mismatch between the substrate and the nucleating phase, it results in a larger nucleation barrier. The inhibition effect can be identified from the increase in the slope and the decrease of the intercept (*cf. curve 0* to *curve 2* in Fig. 3). Therefore, in the following discussion, we can apply these parameters to analyze the effect of the biomolecule on the kinetics of HAP nucleation.

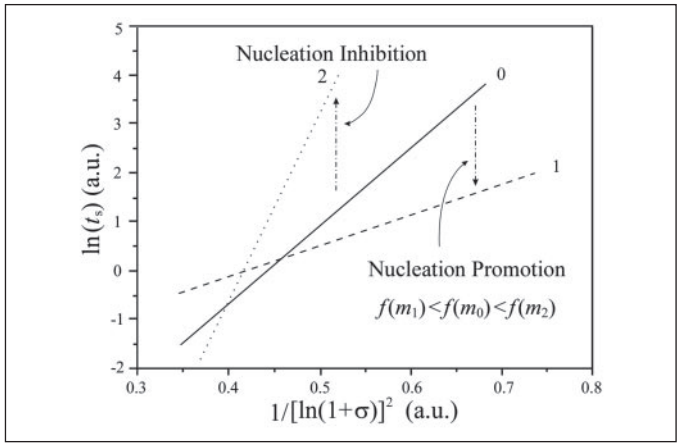

FIGURE 3. **The effect of additives on the interfacial correlation factor *f*(*m*) and the nucleation kinetics.** A promotion or inhibition effect will lower or increase the interfacial correlation factor $f(m)$ in the $\ln(t_s) \sim 1/[\ln(1+\sigma)]^2$ plot. *a.u.*, arbitrary units.

Effect of ChS on the Nucleation Kinetics of HAP—ChS, as the main glycosaminoglycan of tissue and proteoglycan in the extracellular matrix of cartilage and bone, plays an important role in mineralization (18). In nature, biomineralization is a highly complex process. To obtain a good understanding on the rigorous mechanisms of biomineralization, we examined the effect of ChS on the nucleation kinetics of HAP in our experiments, and the results are shown in Fig. 4 and TABLE ONE.

As mentioned earlier, the resultant effect of additives can be decided by the changes of slope and intercept of the line (*cf.* Fig. 3), whether in nucleation promotion or nucleation inhibition. Therefore, we identify in our system the effect of ChS on nucleation and analyze the change of the structure correlation between the HAP crystal and the substrate (including dust, foreign particles, HAP crystallites, etc.) in terms of the variation of the interfacial correlation factor $f(m)$. As shown in Fig. 4*A*, both curves (in the absence of additives and in the presence of ChS) can in principle be fit by two intersecting straight lines with different slopes, which divide the supersaturation space into two regimes at σ^* (or $\sigma^{*\prime}$). The occurrence of two lines indicates that the nucleation is controlled by two values of $f(m)$ within the supersaturation regimes. For the control curve, in regime I, a low value of $f(m_1)$ corresponds to a good structural match, resulting in growing crystals that are well orientated and ordered with respect to the structure of the substrate (29). However, the range of supersaturation in this regime is very narrow. As the supersaturation increases from regime I to II, $f(m)$ increases from $1.05 \times 10^5/\kappa$ to $2.10 \times$

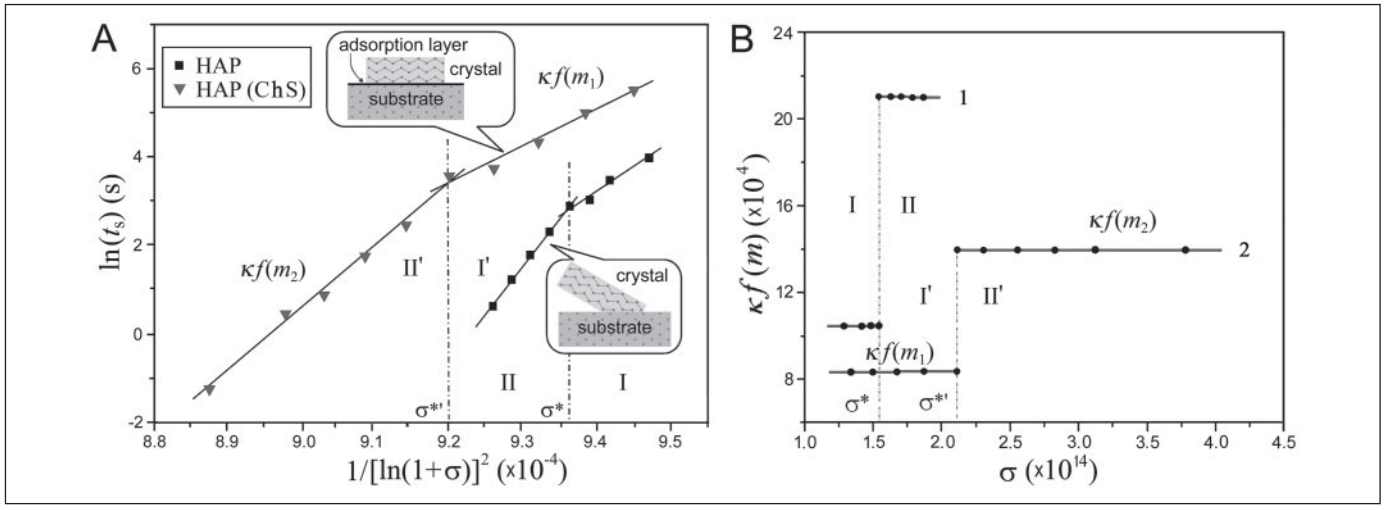

FIGURE 4. *A*, $\ln t_s \sim 1/[\ln(1+\sigma)]^2$ plot for HAP nucleation under the effect of ChS. *B*, plot of $\kappa f(m) \sim \sigma$. The step increase of $\kappa f(m)$ with supersaturation corresponds to the supersaturation-driven interfacial structure mismatch for *curves 1* and *2* in *A*. *Curve 1*, no additive; *curve 2*, 10 mg/liter ChS. The presence of ChS results in a shift of σ^* toward a higher supersaturation.

Downloaded from www.jbc.org at Univ of Ottawa - OCUL, on February 25, 2013

TABLE ONE

Effect of ChS on the interfacial correlation parameters for HAP nucleation

$\kappa f(m)$ is the slope of the corresponding curve. $\sigma^*_{1\to2}$ corresponds to the supersaturation for the transition $f(m_1) \to f(m_2)$.

Additives	$\kappa f(m_1) \times 10^4$	Intercept I	$\kappa f(m_2) \times 10^4$	Intercept II	$\sigma^*_{1\to2} \times 10^{14}$
Deionized water	10.5	−95.2	21.0	−193.9	1.54
ChS (0.001% weight)	8.3	−73.4	14.0	−125.3	2.12

$10^5/\kappa$ (*cf.* Fig. 4*B*), resulting in a mismatch branching emerging on the substrate (Fig. 4*A*, *bottom right inset*). This indicates that an increase in supersaturation tends to drive the interfacial structure correlation between the substrate and HAP from a match state to a mismatch state, *i.e.* the so-called supersaturation-driven interfacial structure mismatch (29).

A comparison with the control curve shows that the presence of ChS results in a decrease in $f(m)$ and an increase in the intercept of the corresponding lines (*cf.* Fig. 4, *A* and *B*), which is in good agreement with the case of nucleation promotion (Fig. 3). This implies that the adsorbed ChS can modify the original substrates and lead to a stronger interaction and a better structural match between the substrate and HAP, which results in an orderly crystallite assembly, albeit at high supersaturation (Fig. 4*A*, *top left inset*). In addition, the factor $f(m_1)$ ($8.3 \times 10^4/\kappa$), referring to regime *I′* and corresponding to nucleation under the influence of ChS, is much lower than that in the control sample in regime I. This indicates that ChS can also lower the nucleation barrier by improving the interfacial structure correlation, especially at low supersaturations (*cf.* Equation 5). Therefore, the nucleation of HAP will be best templated by substrates in this case.

Here, we should highlight an important point; σ^* is shifted to a larger value in the presence of ChS (*cf.* Fig. 4*B*), which corresponds to a larger regime I. This indicates that ChS can stretch the structural match domain toward a much higher supersaturation and suppress the supersaturation-driven structural mismatch. This in turn will facilitate the formation of perfectly aligned HAP assemblies in a larger regime. The effect was verified by our experiments as shown in Fig. 6, to be discussed below. Therefore, this structural match transition effect is extremely important in engineering biomaterials with self-assembled structures.

Nucleation and Growth of Self-assembled HAP Crystallites with the Effect of ChS—For the initial mineralization to occur, the calcium, phosphate, and hydroxyl ions of HAP must come together with the correct orientation and with sufficient energy to form a nucleus. Apart from the above analyses on nucleation kinetics, here we discuss the promotion effect of ChS on self-assembled HAP crystallites from the viewpoints of molecular interfacial structure and properties. Chondroitin 4-sulfate is a linear polysaccharide of repeated disaccharide units (Fig. 1). Such a unit contains sulfate groups and carboxylate groups. The combination of these two functional groups will provide a high density of negative charge. This was verified by a ζ potential measurement. The ζ potential was −38.4 mV for the ChS aqueous solution with a concentration of 100 mg/liter at pH 6. To understand well the electrochemical properties of ChS, we also studied the effect of the calcium ion on the ζ potential of ChS. Fig. 5 shows the ζ potential of ChS as a function of the calcium ion concentration. It is highly negative at low Ca^{2+} concentration, whereas the ζ potential rapidly increases as the concentration increases. The behavior of the ζ potential indicates the strong calcium ion binding of ChS molecules. The reason is that Ca^{2+} is a multivalent cation, which is easily electrostatically bound to the negatively charged surface of ChS. Therefore, adding Ca^{2+} leads to a less negative ζ potential.

To investigate the calcium binding capacity of ChS, equilibrium dialysis was carried out using a microdialyzer system, and the results are shown in Fig. 5*B*. The data obtained from the dialysis enabled us to determine the dissociation constants K_d and the number of binding sites. As shown in the Scatchard plot (Fig. 5*B*, *inset*), ChS exhibits a markedly biphasic Ca^{2+} binding within the Ca^{2+} concentration used. This suggests that ChS contains two Ca^{2+} binding sites with different affinities. These data fit well with the two-site binding model and yielded a high affinity Ca^{2+} binding site (K_d = 2.0 μM) and a modest affinity Ca^{2+} binding site (K_d = 15.2 μM). The result of our dialysis experiment is consistent with previous studies, which indicated that the interaction with calcium is strong for ChS (30, 31). The main binding sites imply the sulfate group and the carboxyl group of the disaccharide units. This position has been identified in salts of chondroitin 4-sulfate (31). Therefore, the presence of molecules will facilitate the nucleation of HAP (Fig. 6*A*) by binding with Ca^{2+} and hence by producing locally a high degree of supersaturation (32, 33).

Binding studies have also demonstrated that ChS can easily bind to HAP, with a semirigid conformation (34, 35). Furthermore, ChS has been shown to bind preferentially to the (100) face of the HAP crystal.

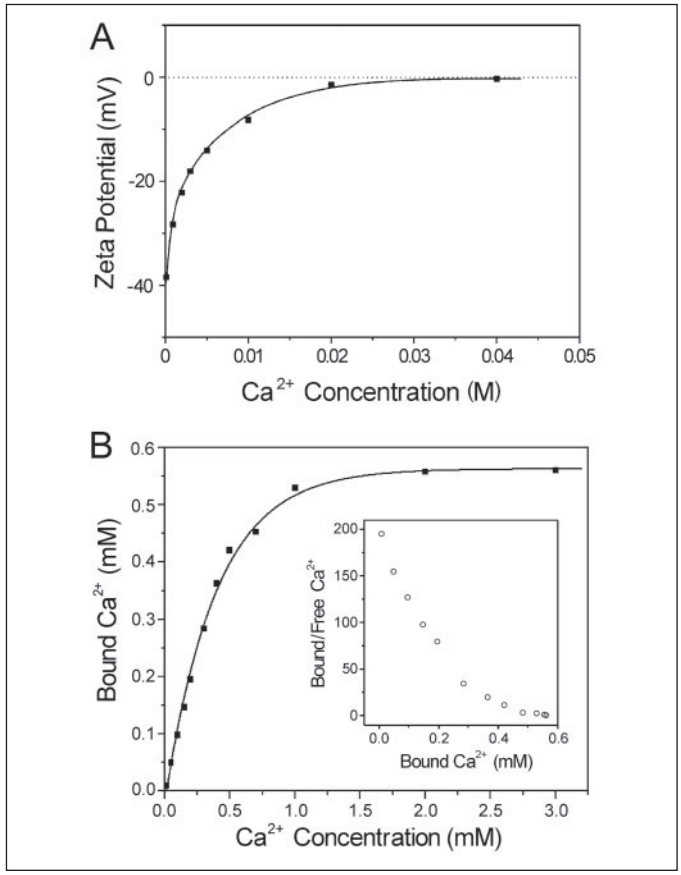

FIGURE 5. **ζ potential measurement and binding of Ca^{2+} to ChS.** *A*, ζ potential *versus* concentration of Ca^{2+} for the ChS aqueous solution. It is largely negative at low Ca^{2+} concentration, whereas the ζ potential increases rapidly with increasing concentration of Ca^{2+}. *B*, Ca^{2+} binding curve of ChS at the concentration of 100 mg/liter determined by equilibrium dialysis with $^{45}Ca^{2+}$. Each point represents the average value of three independent experiments. *Inset*, Scatchard plot for the Ca^{2+} binding capacity of ChS, which indicates that ChS has two Ca^{2+} binding sites.

Downloaded from www.jbc.org at Univ of Ottawa - OCUL, on February 25, 2013

Therefore, once HAP crystallites occur in the solution, ChS will be easily adsorbed on the prism faces of HAP due to its negatively charged surfaces, as shown in Fig. 6*B*.

The adsorption of ChS on the surface of parent HAP crystallites will change the interfacial properties by the functional groups. For instance, the sulfate group plays an important role not only in increasing the stiffness of the molecule but also in creating new binding sites for calcium cations at the substrate. These spatially periodic functional groups, occurring on the surface of the substrate and providing a consistent number of binding sites, could largely lower the nucleation barrier, thus functioning as a template for orientated HAP nucleation. As illustrated in Fig. 6*C*, the favorable binding sites for calcium ions facilitate the formation of additional nuclei (secondary nucleation) on the prism faces of parent crystals. Meanwhile, since ChS has a high and specific affinity for HAP, the nuclei can be stabilized by ChS on the surface of the parent crystallite. Besides, due to the slow surface integration kinetics, the prism faces of the HAP crystallites correspond to a higher surface supersaturation. It follows that epitaxial nucleation and growth can occur on the prism face of HAP.

The nature and strength of the interaction of ChS with HAP and calcium ions has important implications not only in regulating crystal nucleation, but also in regulating the orientation and the size of the growing crystals. Due to the adsorption of ChS on the prism faces of HAP, the negatively charged surface of ChS causes a higher local concentration of Ca^{2+} around the prism faces than in the bulk. Besides, the growth rate of the prism face is much slower than in the axial direction (21). Therefore, those crystallites growing along the prism of parent crystals have a larger growth rate, since they can make the best of the higher surface surpersaturation on the prism faces. As illustrated in Fig. 6*D*, as the nucleation and growth of nuclei proceed further, an orientated HAP assembly will be formed by the growth and coalescence of crystallites on the surface of the modified substrate. In addition, although ChS could initially stabilize the nuclei, the coating of the parent crystals with the macromolecule might block further growth, thereby preventing the formation of large size minerals.

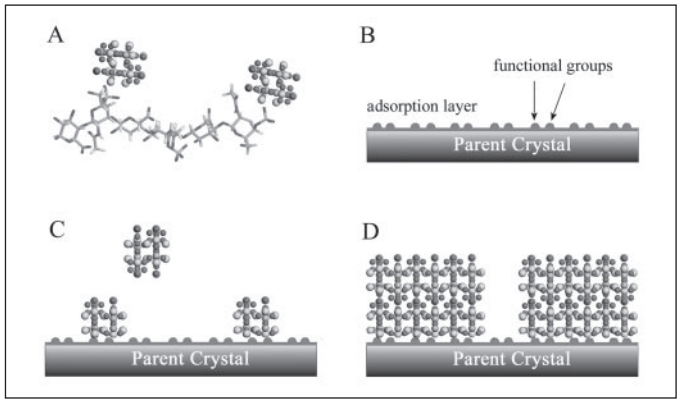

FIGURE 6. **Schematic drawing of the nucleation and growth mechanism of HAP from aqueous solutions with ChS.** *A*, strong interaction between ChS and calcium, which facilitates the nucleation of HAP in solution by producing locally a high degree of supersaturation. *B*, adsorption of ChS on the surface of a parent crystal improving the interfacial correlation. *C*, nucleation and adsorption of growth units on a substrate of ChS. *D*, growth and coalescence of crystallites to form highly orientated HAP crystallites on the surface.

Biomimetic Formation of Self-aligned HAP Nanocrystallites and Implications in Engineering of Mineralized Tissues and Functional Materials—Since evidence from the nucleation kinetics experiments supports the template effect of ChS, we undertook to verify the above analysis and predictions. HAP aggregates were formed from the solutions with and without ChS at the same supersaturation in regime II (*cf.* Fig. 4). By employing a combined electron microscope and electron diffraction technique, we studied their microstructure. As shown in Fig. 7*A*, SE micrographs and especially a higher magnification SE micrograph (*inset*) indicate that needle-like HAP nanocrystallites obtained from the solution in the absence of ChS are assembled in a disordered or random manner. The orientations of the HAP crystallites in porous aggregates are random. This is a consequence of the poor interfacial correlation between HAP and the substrates during the nucleation process, in good agreement with our prediction based on the kinetic analysis. Therefore, the crystallization process in such a case will lead to an open and porous structure due to the supersaturation-driven structural mismatch (29), and we may then obtain porous and brittle tissues in biotechnological applications.

However, the HAP crystallite aggregates formed in the presence of ChS at the same supersaturation show a remarkable difference in microstructure. SE micrographs in Fig. 7*B* reveal a compact and ordered microstructure of HAP assemblies. In each assembly, the HAP nanocrystallites mediated by ChS are aligned parallel to each other. Besides, transmission electron micrographs (Fig. 7*C*) show compact and aligned HAP crystallite assemblies, which are consistent with the SE observations. The microstructure was also confirmed by a selected area electron diffraction pattern (Fig. 7*C*, *top right*) taken from a HAP assembly: the presence and orientation of the diffraction arcs corresponding to the (002) and (004) planes indicate preferential alignment of the HAP crystallites with their *c* axes along the long axis of the bundle. This implies that ChS improved the interfacial structure match between HAP crystallites and substrates during the nucleation process. Therefore, composites such as hard tissues resulting from mineralization under such a condition will become compact, orderly, and tough.

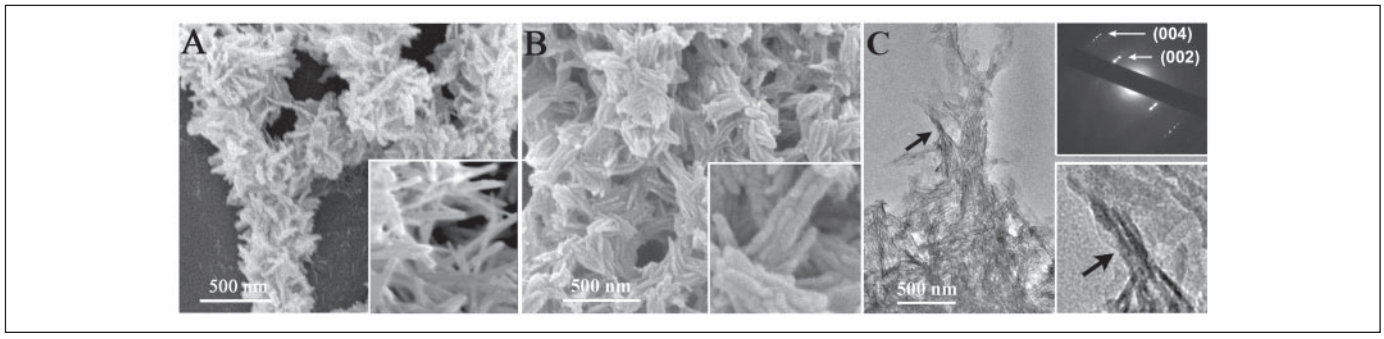

FIGURE 7. *A*, SE micrographs of HAP crystallite aggregates obtained from a solution without additives in regime II (*cf.* Fig. 4). Higher magnification SE micrograph (*inset*) shows disordered and porous HAP aggregates with random orientations. *B* and *C*, SE and transmission electron micrographs of HAP crystallite aggregates obtained from a solution with ChS. Both SE and transmission electron micrographs (*bottom right insets*) show compact and ordered HAP crystallite assemblies. *Top right inset* is a selected area electron diffraction pattern taken from a HAP assembly (*arrow*).

Downloaded from www.jbc.org at Univ of Ottawa - OCUL, on February 25, 2013

The biomimetic formation experiments demonstrate that ChS is capable of facilitating the formation of an ordered HAP assembly by suppressing the supersaturation-driven structural mismatch, as predicted in the kinetics and interfacial structure analysis. In addition, our study on the nucleation kinetics of self-assembly HAP implies wide ranging applications. For example, the role of ChS in the construction of the composites may provide a direct guide for engineering of hard tissues and high performance biomaterials. As we know, natural materials such as bone and tooth are nanocomposites of proteins and minerals with hierarchical structure and superior strength. Based on our study, taking advantage of self-assembled properties, formation of ordered nanobiocomposites could be achieved by means of improving the interfacial structure match by a suitable organic matrix and careful control of conditions such as supersaturation and pH.

In summary, we have studied the nucleation kinetics of HAP and quantified the effect of ChS on HAP nucleation. Both nucleation and biomimetic formation experiments demonstrate that ChS can suppress the supersaturation-driven interfacial structure mismatch and promote the formation of a highly ordered HAP crystallite assembly. The templating effect of ChS on the nucleation of HAP was analyzed not only from the viewpoint of nucleation kinetics but also from the viewpoint of a molecular structure match. These findings will enable us to obtain a better understanding of the fundamentals of the biomineralization of self-assembled hybrid structures and provide important design principles for hard tissue engineering and the development of biocompatible materials.

Acknowledgments—We thank Dr. Zhengjun Li for technical assistance and Dr. Christina S. Strom for valuable discussion and suggestions.

REFERENCES

1. Krampitz, G., and Graser, G. (1988) *Angew. Chem. Int. Ed. Engl.* **27,** 1145–1156
2. Mann, S. (1993) *Nature* **365,** 499–505
3. Weiner, S., Addadi, L., and Wagner, H. D. (2000) *Mater. Sci. Eng. C* **11,** 1–8
4. Stupp, S. I., and Braun, P. V. (1997) *Science* **277,** 1242–1248
5. Weiner, S., and Addadi, L. (1997) *J. Mater. Chem.* **7,** 689–702
6. Kjellen, L., and Lindahl, U. (1991) *Annu. Rev. Biochem.* **60,** 443–475
7. Colfen, H., and Mann S. (2003) *Angew. Chem. Int. Ed.* **42,** 2350–2365
8. Bauerein, E. (2003) *Angew. Chem. Int. Ed.* **42,** 614–641
9. Snead, M. L. (2003) *Connect. Tissue Res.* **44,** 47–51
10. Wilt, F. H., Killian, C. E., and Livingston, B. T. (2003) *Differentiation* **71,** 237–250
11. Greenfield, G., Wilson, D. C., and Crenshaw, M. A. (1984) *Am. Zool.* **24,** 925–932
12. Mann, S. (1988) *Nature* **332,** 119–124
13. Addadi, L., and Weiner, S. (1985) *Proc. Natl. Acad. Sci. U. S. A.* **82,** 4110–4114
14. Veis, A. (1989) in *Biomineralization: Chemical and Biochemical Perspectives* (Mann, S., Webb, J., and Williams, R. J. P., eds) pp. 189–216, VCH Publishers, New York
15. Albeck, S., Weiner, S., and Addadi, L. (1996) *Chem. Eur. J.* **2,** 278–284
16. Rajamani, L., Kini, R. M., and Suresh, V. (2003) *Proc. Natl. Acad. Sci. U. S. A.* **99,** 5155–5159
17. Embery, G., Hall, R., Waddington, R., Septier, D., and Goldberg, M. (2001) *Crit. Rev. Oral Biol. Med.* **12,** 331–349
18. Goldberg, M., Rapoport, O., Septier, D., Palmier, K., Hall, R., Embery, G., Young, M., and Ameye, L. (2003) *Connect. Tissue Res.* **44,** 184–188
19. Paroli, E., Antonilli, L., and Biffoni, M. (1991) *Drugs Exp. Clin. Res.* **17,** 9–19
20. Moss, M., Kruger, G. O., Reynolds, D. C. (1965) *Oral Surg. Oral Med. Oral Pathol.* **20,** 795–801
21. Liu, X. Y. (2001) *Advances in Crystal Growth Research* (Sato, K., Nakajima, K., and Furukawa, Y., eds) pp. 42–61, Elsevier Science, Amsterdam
22. Elliott, J. C. (1994) *Structure and Chemistry of the Apatites and Other Calcium Orthophosphates*, pp. 9–50, Elsevier Science, Amsterdam
23. Scatchard, G. (1949) *Ann. N.Y. Acad. Sci.* **51,** 660–672
24. Mutaftschiev, B. (1993) *Handbook of Crystal Growth*, pp. 187–248, North-Holland, Amsterdam
25. Zettlemoyer, A. C. (1969) *Nucleation*, pp. 225–307, Dekker, New York
26. Liu, X.Y. (2000) *J. Chem. Phys.* **112,** 9949–9955
27. Jiang, H. D., and Liu, X. Y. (2004) *J. Biol. Chem.* **279,** 41286–41293
28. Liu, X. Y. (2000) *Langmuir* **16,** 7337–7345
29. Liu, X. Y., and Lim, S. W. (2003) *J. Am. Chem. Soc.* **125,** 888–895
30. Rodriguez-Carvajal, M. A., Imberty, A., and Perez, S. (2003) *Biopolymers* **69,** 15–28
31. Millane, R. P., Mitra, A. K., and Arnott, S. (1983) *J. Mol. Biol.* **169,** 903–920
32. Lindahl, U., and Hook, M. (1978) *Annu. Rev. Biochem.* **47,** 385–419
33. Hunter, G. K., and Bader, S. M. (1989) *J. Theor. Biol.* **138,** 195–211
34. Rees, S. G., Wassell, D. T. H., and Embery, G. (2002) *Biomaterials* **23,** 481–489
35. Hall, R., Embery, G., Waddington, R., and Gilmour, A. (1995) *Calcif. Tissue Int.* **56,** 236–239

Downloaded from www.jbc.org at Univ of Ottawa - OCUL, on February 25, 2013